ingegneria sismica
International Journal of Earthquake Engineering
Anno XLIII - Num. 2 - 2026

Effect of electrical discharge machining parameters on the microstructure of DD9 single crystal superalloy

Shuai Zheng[1,2,*] *and Yulan Zhu*[1,2]

[1] Science and Technology on Advanced High Temperature Structural Materials Laboratory, AECC Beijing Institute of Aeronautical Materials, Beijing 100095, China
[2] High Temperature Structure Materials Di-vision, AECC Beijing Institute of Aeronautical Materials, Beijing 100095, China

SUMMARY: *To reveal the influence of electrical discharge machining (EDM) parameters on the pore wall microstructure of DD9 single crystal high-temperature alloy, this paper takes 2404554MICRO01 to MICRO05 series specimens as objects, and conducts 500 × microscopic observation and recast layer measurement on five sets of circular and horn holes, B119, B222, B716, B1503, and B1902. Extract 10 thickness measurement points for each operating condition, calculate the average thickness, maximum thickness, coefficient of variation, and local instability index. The results showed that the average thickness of the recast layer of the circular hole increased from 6.0 μ m to 16.4 μ m, and the maximum thickness of the B1503 circular hole reached 44 μ m, with a local instability index of 2.68. The average thickness of the horn hole under B119 is 9.1 μ m, and the coefficient of variation of the horn hole under B222 is 77.45%. Mechanism analysis shows that pulse heat input controls overall thickening, hole geometry amplifies local non-uniformity through discharge gaps and flushing disturbances, and the γ/γ 'structure affects the re solidification interface and microcrack initiation.*

KEYWORDS: *Electrical discharge machining; DD9 single-crystal superalloy; recast layer; flared hole; microstructure evolution*

1 Introduction

The DD9 single crystal high-temperature alloy possesses high temperature strength, creep resistance, and organizational stability, making it an important candidate material for advanced aircraft engine turbine blades, guide vanes, and other heat-end load-bearing components. For such components, the material's own high-temperature properties alone cannot solely determine the service reliability; the processing quality of air film cooling holes, micro channels, and special-shaped holes also directly affects the local cooling efficiency, thermal stress distribution, and crack initiation location. Especially in single crystal blades, the cooling holes are often located in the area where the gas is subjected to high-temperature gas scouring, thermal mechanical fatigue, and oxidation corrosion. Once a thick casting layer, micro cracks, or recrystallization defects form near the hole wall, they may become the preferred channels for fatigue damage and oxidation invasion. Electrical Discharge Machining (EDM) utilizes the instantaneous high temperature generated by pulsed discharge to remove the material and can produce small-sized and complex-shaped hole structures on

*zhengs2035@163.com
https://doi.org/10.65102/is2026857
Published: 30 April, 2026

high-strength, difficult-to-machine high-temperature alloys like DD9, thus having obvious applicability in micro-hole and air film hole processing. However, the advantages of EDM are accompanied by typical thermal damage issues: the metal on the hole wall melts under the action of discharge heat, some molten metal is carried away by the working fluid, and the remaining part rapidly solidifies in a very short time, forming a recast layer with a significantly different microstructure from the base material. Existing research on air film holes in single crystal high-temperature alloys indicates that the formation of the recast layer around the hole is closely related to transient melting, rapid solidification, and the thermal influence on the hole wall, and its thickness and continuity affect the surface integrity of the hole wall [1]. Therefore, for the DD9 single crystal high-temperature alloy, the quality control of EDM hole drilling cannot be limited to the hole diameter or macroscopic morphology, but should further focus on the micro-structural responses caused by the discharge parameters.

In recent years, research on EDM or wire electrical discharge machining (WEDM) has mainly concentrated on Inconel 718, Inconel 690, Hastelloy, and other nickel-based high-temperature alloys. For example, the WEDM processing of Inconel 718 has systematically characterized the formation characteristics of the recast layer and pointed out that this layer is usually accompanied by droplets, holes, microcracks, and surface roughening [2]; parameter optimization studies have also shown that input variables such as pulse current, pulse width, pulse interval, and wire speed simultaneously affect the material removal rate, surface roughness, and processing stability [3]. For Inconel 718 obtained from different forming paths, the surface integrity of WEDM is also affected by the initial microstructure characteristics, indicating a coupling relationship between the base microstructure and the discharge response [4]. Additionally, multi-objective optimization and regression analysis have been used to balance processing efficiency, surface quality, and energy consumption [5]. The Inconel 690 micro-gear processing research also shows that response surface methods and artificial neural networks can be used to predict WEDM processing performance [6]. Research on Ni-Cu high-temperature alloys further indicates that WEDM input variables have a significant impact on the machinability of difficult-to-machine alloys [7], while the RSM-GRA optimization results of Inconel 690 suggest that a single evaluation index is difficult to fully reflect the quality of EDM processing [8]. At the same time, studies on the use of renewable media for processing Inconel 718 [9] and the use of alumina nanofluids for powder mixing EDM [10] have shown that the working medium and discharge environment also change the processing heat input and surface morphology. Although the above studies have provided an important foundation for EDM/WEDM processing of nickel-based alloys, their subjects are mostly polycrystalline or additive manufacturing nickel-based alloys. There is still insufficient discussion on the quantitative relationship between "discharge parameters - hole shape differences - recast layer thickness - microstructure damage" in DD9 single crystal high-temperature alloys. Especially, there are significant differences in chip removal paths, fluid conditions, hole mouth heat accumulation and secondary discharge probability between round holes and conical holes. Only using average surface roughness or a single processing efficiency indicator to explain the quality of hole formation is difficult to reveal the true source of microstructure damage on the hole wall.

Based on the above problems, this paper takes the 2404554MICRO01–2404554MICRO05 series DD9 single crystal high-temperature alloy specimens as the research object, and conducts microstructure comparisons around processing numbers such as B119, B222, B716, B1503 and B1902 for round holes and conical holes. The research focus is not simply to display the micrographs of different hole types, but to convert the 500× microstructure images into comparable recast layer thickness data and evidence of hole wall damage. Specifically, this paper will identify the recast layer boundaries on the hole wall through cross-sectional

microscopic observation, measure the local thickness at different measurement points, and calculate the average thickness, maximum thickness and thickness dispersion; at the same time, combining the hole mouth morphology and microcrack distribution, determine the heat influence intensity under different EDM parameter combinations. The round hole samples are mainly used to evaluate the benchmark recast layer characteristics under relatively stable discharge channels, while the conical hole samples are used to analyze the possible local heat concentration, molten metal re-deposition and non-uniform solidification of the hole mouth expansion structure. By comparing the round hole samples and conical hole samples of the same processing number in pairs, this paper can more clearly distinguish the parameter effect from the hole type effect, and avoid misjudging the hole wall damage caused by geometric factors as a simple discharge energy difference.

The main contributions of this paper are reflected in four aspects. Firstly, a quantitative measurement process for recast layers after EDM hole formation in DD9 single crystal high-temperature alloys is established, making microstructure photos no longer just qualitative evidence but capable of supporting thickness statistics and parameter comparison. Secondly, the microstructure differences between round holes and conical holes under the same processing number are compared, highlighting the influence of hole type geometry on chip removal, fluid conditions and local secondary discharge. Thirdly, the recast layer thickness, maximum local damage, microcrack characteristics, hole mouth geometry and EDM parameters are included in the same analysis framework, thereby forming an explanatory chain from process input to tissue response. Finally, the research results can provide experimental basis for optimizing the EDM process window of DD9 single crystal blade microholes and special-shaped holes, especially helpful in determining the balance range between low recast layer thickness, low microcrack risk and good hole mouth integrity. Different from studies that only focus on material removal rate or surface roughness, this paper emphasizes the constraining effect of microstructure integrity on the safety of high-temperature service, thus providing more engineering-oriented evidence for the quality evaluation of complex hole processing in single crystal high-temperature alloys.

2 Methods

2.1 Materials, EDM Parameter Matrix, and Hole Geometry Grouping

This study selected DD9 single-crystal high-temperature alloy as the experimental material, and the research object was the microstructure changes in the hole wall area after electrical discharge machining. DD9 belongs to a typical nickel-based single-crystal high-temperature alloy. The material has high organizational stability and creep resistance under high-temperature bearing conditions, but its high strength, high hardness, and low thermal conductivity also make traditional mechanical hole-making prone to problems such as tool wear, hole wall deformation, and processing thermal damage [11, 12]. Therefore, this paper uses the electrical discharge machining method to prepare round holes and flared holes, and takes the microstructure of the hole wall section as the evaluation object, focusing on analyzing the morphology, thickness changes of the recast layer, and local thermal influence characteristics at the hole opening under different processing numbers [13].

The experimental samples include five groups of DD9 single-crystal high-temperature alloy samples: 2404554MICRO01, 2404554MICRO02, 2404554MICRO03, 2404554 MICRO04, and 2404554MICRO05. After EDM hole-making, each sample was sectioned and observed under metallographic microscopy to obtain the morphology of the recast layer near the hole wall. To ensure the comparability of different samples, all microstructure images

were captured at a magnification of 500×, and the same section observation direction, image scale calibration method, and thickness measurement criteria were maintained [14]. This paper does not regard a single micrograph as an isolated evidence, but includes each group of images in a unified sample number, processing number, hole type, and response index system for comparison.

The processing numbers include B119, B222, B716, B1503, and B1902. Each processing number corresponds to a set of EDM parameter combinations, with the main parameters including peak current, pulse width, pulse interval, open-circuit voltage, servo gap, electrode material, flushing pressure, and processing polarity [16]. Among them, the peak current and pulse width mainly determine the instantaneous heat input during a single discharge process [15]. The pulse interval affects the cooling of molten metal, chip removal, and the recovery of the working fluid insulation state. The open-circuit voltage and servo gap affect the stability of the discharge channel. The electrode material and processing polarity will change the electrode wear, the proportion of heat distribution, and the material removal behavior of the hole wall [16]. The flushing pressure affects the efficiency of the molten product discharge and the probability of secondary discharge in the hole. These parameters jointly determine the formation of the molten layer on the hole wall, the degree of recrystallization, and the intensity of local tissue damage.

To highlight the influence of hole type geometry on the EDM microstructure response, this paper divides the hole type into two categories: round hole and flared hole. The round hole represents the relatively conventional straight hole processing structure, mainly used to evaluate the thickness and continuity of the recast layer under stable hole wall discharge conditions [17]. The flared hole has an expansion feature at the hole opening, and its local geometric changes may cause disturbances in the flushing flow field, heat accumulation in the hole opening area, and fluctuations in the discharge position, making it more suitable for analyzing the re-melting, re-deposition, and thickness non-uniformity phenomena at the edge of the hole opening in the processing of irregular holes [18]. For the same processing number, the round hole and the flared hole form a paired comparison relationship, which can be used to distinguish the relative influence of parameter changes and hole type changes on the microstructure. The specific EDM processing parameters and grouping are shown in Table 1.

Table 1: EDM Machining Parameters and Grouping.

Group	Specimen ID	Hole geometry	Machining code	Main microstructural responses
1	2404554MICRO01	Round hole	B119	Average recast layer thickness, maximum thickness, microcrack density
	2404554MICRO01	Flared hole	B119	Recast layer continuity, edge thermal damage
2	2404554MICRO02	Round hole	B222	Average and maximum recast layer thickness
	2404554MICRO02	Flared hole	B222	Thickness variation, edge resolidification
3	2404554MICRO03	Round hole	B716	Recast layer uniformity, local microcracks
	2404554MICRO03	Flared hole	B716	Hole edge thermal accumulation
4	2404554MICRO04	Round hole	B1503	Recast layer continuity
	2404554MICRO04	Flared hole	B1503	Flared-edge remelting feature
5	2404554MICRO05	Round hole	B1902	Maximum local damage, microcrack density
	2404554MICRO05	Flared hole	B1902	Edge redeposition and recast-layer variation

In Table 1, the five groups of DD9 single crystal high-temperature alloy specimens are sorted according to the processing number and hole type. Each processing number includes two types of hole types: round hole and flared hole, which are used to compare the influence of the geometric changes of the hole opening on the morphology of the remelt layer and the thermal damage of the hole wall under the same processing conditions. Each sample is observed under a magnification of 500× for microstructure examination. The main response indicators include the average remelt layer thickness, the maximum remelt layer thickness, the thickness dispersion coefficient, the microcrack density, the continuity of the remelt layer, and the thermal damage characteristics at the hole opening edge. Among them, the average remelt layer thickness is used to reflect the overall thermal damage level of the hole wall. The maximum remelt layer thickness is used to capture the local severely re-solidified area [19]. The thickness dispersion coefficient is used to evaluate whether the remelt layer is uniformly distributed along the hole wall. The microcrack density is used to determine the crack tendency under rapid solidification contraction and thermal stress. The continuity of the remelt layer is used to distinguish between complete coverage, local discontinuity, and peeling and other morphological states. The thermal damage characteristics at the hole opening edge are used to evaluate whether there are obvious secondary discharge, droplet adhesion, or edge ablation phenomena in the trumpet-shaped area [20].

The actual EDM parameters are uniformly archived in the experimental records, including peak current, pulse width, pulse interval, open-circuit voltage, servo gap, electrode material, flushing pressure, and processing polarity. If there are repeated processing or multi-field observations in the actual process records, the original measurement values of each field should be retained, and the mean and dispersion degree should be calculated again during the statistics. This can reduce the influence of the selection of a single field on the result judgment and also provide a more stable data basis for the subsequent discussion on the influence of EDM parameters on the microstructure of the hole wall of DD9 single crystal high-temperature alloy.

2.2 Metallographic Preparation and Recast-Layer Quantification

In order to obtain the microstructure information of the hole wall of DD9 single-crystal high-temperature alloy after EDM drilling, this paper conducted cross-sectional sampling, metallographic preparation, and quantitative measurement of the recast layer for each group of samples. The sampling positions were determined based on the characteristics of the hole type: for round holes, the cross-section was preferentially taken along the axial direction passing through the center of the hole to ensure that the recast layers on both sides of the hole wall could be fully observed; for flared holes, the cross-section should cover both the expansion zone at the hole opening and the inner wall transition zone, so that the heat affected zone at the hole edge, local recrystallization, and the thickness change of the hole wall could be presented on the same observation surface [21]. During the cutting process, a low-speed diamond cutting wheel was used, combined with coolant to reduce the secondary influence of mechanical cutting heat on the microstructure of the hole wall. After the cutting was completed, the samples were embedded and marked with the observation direction to ensure that the subsequent micrographs could correspond to the processing number, hole type, and hole opening position.

The metallographic preparation was carried out in the order of rough grinding, fine grinding, and mechanical polishing. The rough grinding stage mainly removed the deformation layer from the cutting and the uneven areas of the cross-section, and the fine grinding stage gradually reduced the grit size of the sandpaper to keep the cross-sectional contour of the hole wall clear. The polishing stage used diamond suspension liquid or oxide

polishing liquid to obtain a low scratch surface. Since the thickness of the recast layer is usually at the micrometer scale, insufficient polishing would cover the recast layer boundary, and excessive polishing might weaken the edge features of the hole wall. Therefore, each sample after polishing should first undergo low-magnification pre-observation to confirm that there were no obvious dragging, collapse, or residue of contaminants in the hole wall area. For areas with a thick re-crystallization layer or adhered hole opening droplets, it should be avoided to peel off artificially during sample preparation to prevent affecting the judgment of the recast layer thickness [22].

The microstructure manifestation was achieved using a chemical corrosion method suitable for Ni-based single-crystal high-temperature alloys. The purpose of the corrosion was to enhance the contrast between the γ/γ′ microstructure, the matrix, and the recast layer, so that the re-crystallization layer boundary of the hole wall could be stably identified [24]. The corrosion time should be adjusted according to the surface reaction of the sample. Too short a time would cause the interface to be blurred, while too long a time might expand the dark etched area at the hole edge and affect the measurement results. After the corrosion was completed, the samples were washed with deionized water and anhydrous ethanol, and then observed immediately after drying. All micrographs used for quantitative measurement were collected at a magnification of 500×, and clear scales, hole wall boundaries, and the outer edge of the recast layer should be retained in the images, avoiding selecting edge-blurred or unevenly bright fields.

Image measurement could be completed using ImageJ, Image-Pro Plus, or the analysis software built into the microscope. Before measurement, the spatial calibration was carried out using the image scale, and the pixel size was converted to the actual length unit. At least 30 equidistant measurement points were selected along the hole wall direction for each micrograph, and the measurement lines should be as perpendicular as possible to the local tangent direction of the hole wall, extending from the outer surface of the recast layer to the junction of the recast layer and the matrix. For continuous recast layers with clear boundaries, the local thickness was directly recorded. For areas with significant undulating boundaries or discontinuous regions, the actual measurement point results should be retained, and the continuity changes of the morphology should be described. If there were microcracks in the same field of view, the number, length direction, and location of the cracks should be recorded, and converted to the microcrack density per unit hole wall length.

To establish a corresponding relationship between EDM parameters and microstructure changes, this paper first calculated the effective discharge energy per pulse. This indicator is used to characterize the effective heat transferred by a single discharge event to the workpiece and can explain the melting depth of the hole wall and the formation trend of the recast layer [25]. The calculation of the effective discharge energy per pulse E_p is shown in Equation (1).

$$E_p=\eta U_g I_p t_{on} \tag{1}$$

In Equation (1), η represents the energy utilization coefficient. U_g represents the discharge gap voltage. I_p represents the peak current. t_{on} represents the pulse width. When the peak current or pulse width increases, the local melting range of the hole wall usually expands, and the possibility of thickening of the recast layer also increases. Subsequently, the duty cycle and pulse frequency are introduced to describe the thermal input rhythm during the continuous discharge process, as shown in Equation (2).

$$D=\frac{t_{on}}{t_{on}+t_{off}} \tag{2a}$$

$$f=\frac{1}{t_{on}+t_{off}} \tag{2b}$$

In Equation (2), D represents the duty cycle, f represents the pulse frequency, and t_{off} represents the pulse interval. The duty cycle reflects the proportion of the discharge time within a pulse cycle, while the pulse frequency indicates the number of discharge events occurring per unit time. A higher duty cycle will subject the pore wall to more intense thermal effects, while shorter pulse intervals may reduce the time for the expulsion of molten products and the restoration of the insulating state of the working fluid. Finally, the thickness and dispersion of the recast layer in each microscopic photograph are statistically analyzed, as shown in Formula (3).

$$\overline{\delta}_{RL}=\frac{1}{n}\sum_{i=1}^{n}\delta_i \tag{3a}$$

$$s_{RL}=\sqrt{\frac{1}{n\text{-}1}\sum_{i=1}^{n}\left(\delta_i\text{-}\overline{\delta}_{RL}\right)^2} \tag{3b}$$

$$CV_{RL}=\frac{s_{RL}}{\overline{\delta}_{RL}}\times 100\backslash\% \tag{3c}$$

In Equation (3), $\overline{\delta}_{RL}$ represents the average remelted layer thickness. δ_i represents the local remelted layer thickness at the i-th measurement point. n represents the number of measurement points. s_{RL} represents the standard deviation of the remelted layer thickness. CV_{RL} represents the coefficient of variation of the remelted layer thickness. This paper also records the maximum thickness in each microscopic photograph, which is used to identify whether there is abnormal heat accumulation in the local area of the hole wall or hole opening. Through the above measurement methods, the 500× microscopic microstructure photographs can be transformed into comparable data such as average thickness, maximum thickness, standard deviation, coefficient of dispersion, and micro-crack density, providing a basis for the subsequent analysis of the tissue differences under processing numbers B119, B222, B716, B1503, and B1902. The schematic diagram of the preparation and quantitative re-melting layer of the metallographic samples of DD9 single crystal high-temperature alloy processed by EDM is shown in Figure 1.

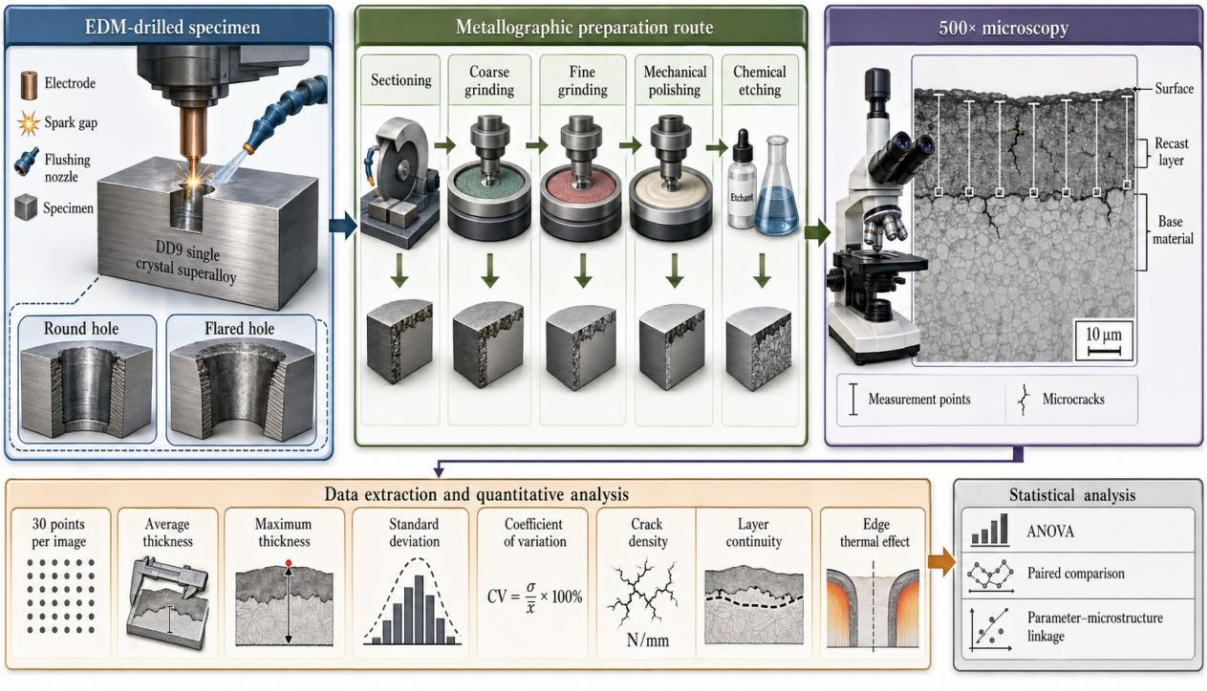

Figure 1: Schematic diagram of metallographic preparation and quantitative re-casting layer of DD9 single-crystal high-temperature alloy processed by EDM.

As shown in Figure 1, after the EDM drilling of round hole and flared hole was completed for the DD9 single crystal high-temperature alloy sample, the sample was first cut along the axial direction of the hole or the key section of the hole opening. Then, the following processes were sequentially carried out: rough grinding, fine grinding, mechanical polishing and chemical etching, in order to expose the γ/γ′ structure near the hole wall and the interface of the remelt layer. On this basis, microscopic structure photos were collected, and the image analysis software calibrated with the ruler was used to measure the thickness at multiple points along the hole wall.

2.3 Statistical Comparison and Parameter–Microstructure Correlation

To enhance the reproducibility and statistical credibility of microstructure analysis, this paper further establishes a quantitative comparison method between the thickness of the recast layer and the process variables of EDM. For the samples 2404554MICRO01 to 2404554MICRO05, at least 30 equidistant measurement points were selected along the hole wall direction for each 500× microstructure photograph. The measurement positions covered the area near the hole opening, the middle area of the hole wall, and the regions with more obvious fluctuations of the local recast layer. Since this paper involved 10 round hole and flared hole microstructure photographs, the final thickness measurement data were no less than 300. When arranging the measurement points, the same image calibration method and thickness determination criteria were maintained as much as possible to reduce the influence of human point selection differences on the statistical results.

During the data processing, round hole and flared hole were separately counted. For each processing number, the average recast layer thickness, standard deviation, maximum recast layer thickness, and coefficient of variation were calculated. The average value was used to characterize the overall thermal damage level of the hole type under the corresponding EDM parameter conditions, the standard deviation and coefficient of variation were used to evaluate the thickness fluctuation of the recast layer along the hole wall direction, and the maximum

value was used to identify whether there were severe recrystallization in the hole opening or the middle area of the hole wall. For the microcracks identifiable in the micrographs, the number of cracks and the effective statistical length were recorded simultaneously, and converted into microcrack density. If there were multiple fields of view for the same hole type, the single field data were first retained, and then the comprehensive statistical results of the hole type were calculated to avoid the excessive influence of a single representative image on the conclusion.

The thickness differences of the recast layer between different processing numbers were tested using one-way Analysis of Variance (ANOVA). The analysis objects included the average thickness data of five processing numbers: B119, B222, B716, B1503, and B1902. If the ANOVA results showed significant differences between the groups, further multiple comparisons were conducted to determine which processing numbers mainly caused the thickness differences. For round hole and flared hole of the same B number, paired comparison was used for hole type comparison. When the data approximately followed a normal distribution, paired t-test was used. When the thickness data were skewed or the sample size was small, the Wilcoxon signed-rank test was used as a robust test method. This comparison was used to determine whether the flared geometry caused more obvious heat accumulation at the hole opening, thickness fluctuation, or edge re-deposition.

In the parameter correlation analysis, this paper used single-pulse effective discharge energy, duty cycle, pulse frequency, fluid pressure, and hole type as the main explanatory variables, and the average recast layer thickness, maximum recast layer thickness, coefficient of variation, and microcrack density as the response indicators. The single-pulse effective discharge energy reflects the intensity of the thermal effect of a single pulse discharge on the hole wall area, and is usually related to the local melting depth and thickening of the recast layer. The duty cycle is related to the proportion of continuous heat input, and can affect the cooling of the hole wall and the discharge of molten products. The pulse frequency describes the frequency of pulse action per unit time, and may change the heat accumulation in the hole and the probability of secondary discharge. The fluid pressure mainly affects the discharge efficiency of molten metal, debris, and discharge products. The hole type factor is used to distinguish the differences in the flow field, discharge gap, and heat effect at the hole opening between the straight hole wall and the flared expansion area. If the subsequent experimental conditions permit, Scanning Electron Microscopy (SEM) and Energy Dispersive Spectroscopy (EDS) analyses can be conducted on representative samples. SEM can be used to observe the micropores, microcracks, droplet adhesion, and recrystallization morphology on the recast layer surface; EDS can be used to analyze whether there is element segregation, oxide inclusions, or processing medium residues between the recast layer and the substrate. For DD9 single crystal superalloy, if there are obvious oxygen enrichment, local segregation of strengthening elements, or discontinuous crack bands in the recast layer, it can further illustrate that the EDM parameters not only change the thickness characteristics of the pore walls but also affect the chemical uniformity of the recrystallization structure and the subsequent service stability. Through the above statistical and characterization methods, the micrographs can be transformed into comparable evidence such as thickness, cracks, and element distribution, providing a data basis for discussing the influence of different EDM parameters on the microstructure of DD9 single crystal superalloy in the result section.

3 Results and Discussion

3.1 Morphology of the recast layer in round and flared holes

To compare the morphology of the recast layer on the hole walls of round holes and flared holes under the processing conditions of B119 and B222, this paper conducted a comparative analysis of their 500× microscopic structure photos, as shown in Figure 2.

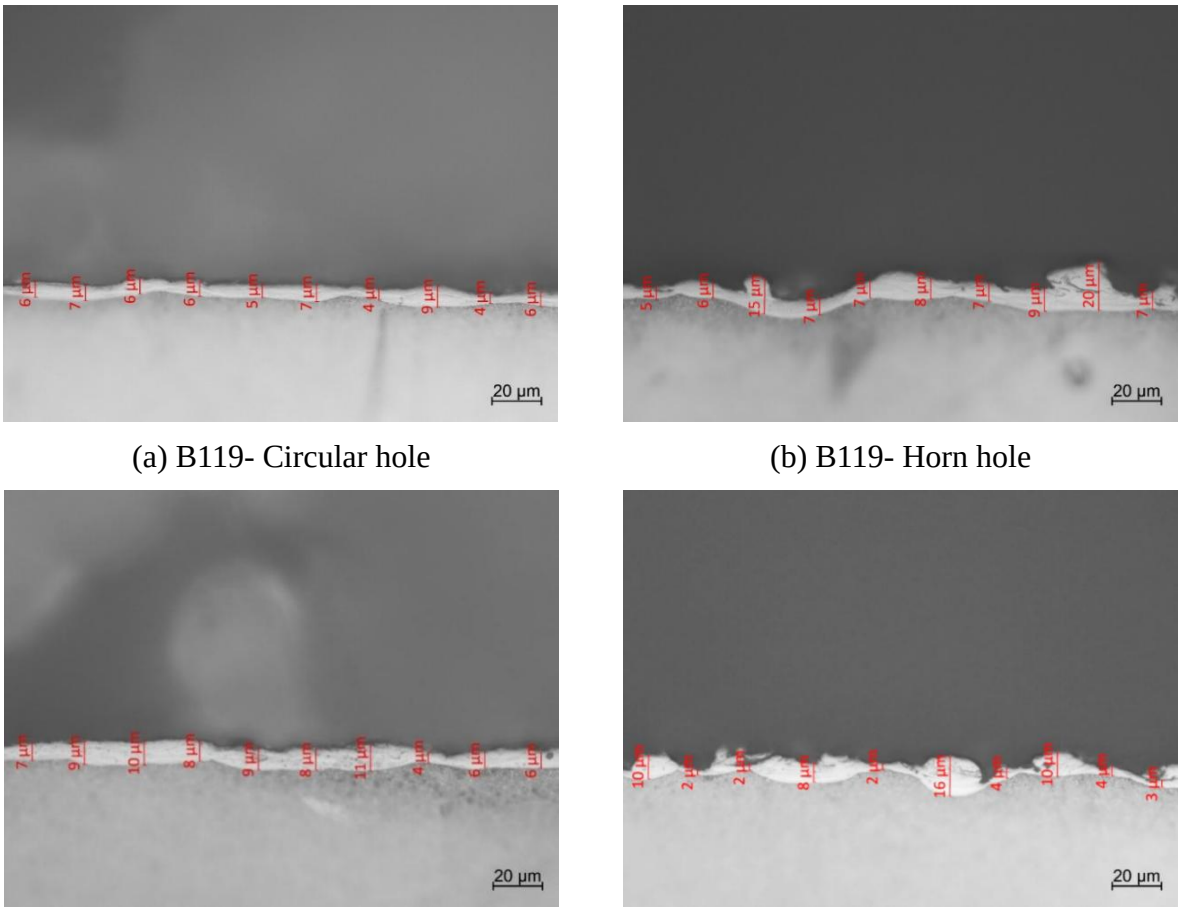

(a) B119- Circular hole (b) B119- Horn hole

(c) B222- Circular hole (d) B222- Horn hole

Figure 2: Recast layer morphology of B119 and B222 holes at 500×.

As shown in Figure 2, light-colored recast layers distributed along the four hole walls can be observed in all the hole wall cross-sections, indicating that the DD9 single crystal superalloy underwent local melting and rapid solidification during the EDM hole-making process. Figure 2(a) is the B119 circular hole, and the thickness of the recast layer marked in the figure is mainly distributed between 4-9 μm. Calculated based on 10 marked measurement points, the average value is approximately 6.0 μm. The recast layer on the hole wall is relatively thin and the interface is relatively straight. Figure 2(b) is the B119 trumpet-shaped hole, the thickness marked values are distributed between 5-20 μm, the average value is approximately 9.15 μm, the maximum measurement point reaches 20 μm, which is significantly higher than that of the same group of circular holes, and there is a local bulging recast zone on the hole wall surface. This indicates that the trumpet-shaped hole area of B119 under this condition is subjected to stronger local heat action, and the phenomenon of molten metal re-deposition is more obvious. Figure 2(c) is the B222 circular hole, the thickness is

mainly concentrated between 6-11 μm, the average value is approximately 8.0 μm, the continuity of the recast layer on the hole wall is relatively good, but the thickness is slightly increased compared to the B119 circular hole. Figure 2(d) is the B222 trumpet-shaped hole, the thickness range is 2-16 μm, the average value is approximately 6.1 μm, although the average thickness is lower than that of the B222 circular hole, the local measurement point reaches 16 μm, and the thickness fluctuates greatly at different positions, reflecting the uneven distribution of the recast layer on the hole wall surface. These results indicate that the B119 group trumpet-shaped holes show higher average thickness and greater local thickening, while the B222 group trumpet-shaped holes exhibit stronger thickness dispersion, indicating that the influence of the die shape on the recast layer morphology changes with the processing number. On the basis of the B119 and B222 groups, further observation of the microstructure of the hole walls of the B716 and B1503 groups is helpful for judging whether more obvious thickening, discontinuity or enhanced heat influence at the hole opening occurs in the recast layer morphology under subsequent processing numbers, as shown in Figure 3.

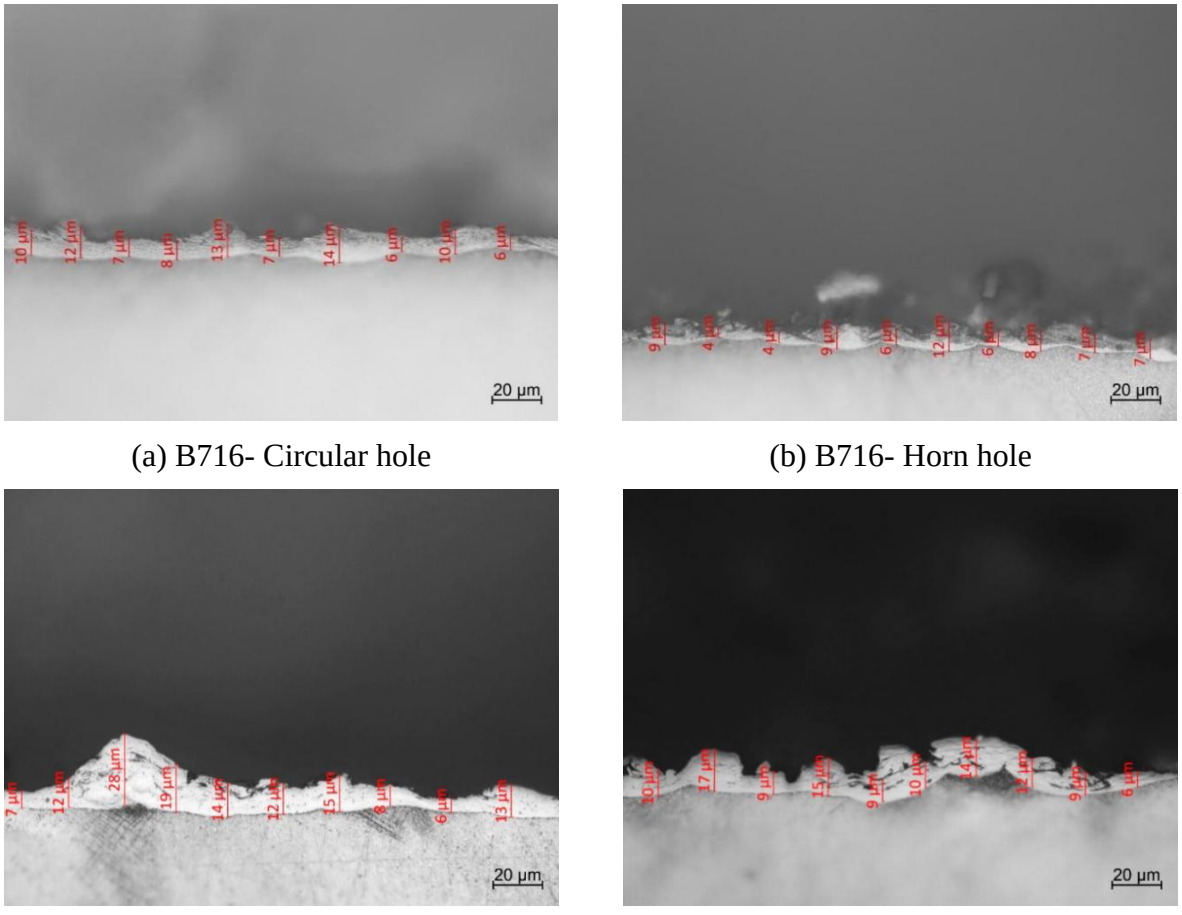

(a) B716- Circular hole (b) B716- Horn hole

(c) B1503- Circular hole (d) B1503- Horn hole

Figure 3: Recast layer morphology of B716 and B1503 holes at 500×.

As shown in Figure 3, the recast layer of the B716 group still mainly consists of continuous thin layers. In Figure 3 (a), the marked thickness of the B716 circular holes is 6–14 μm, with an average value of approximately 9.3 μm. The surface of the hole wall is relatively smooth, with only slight undulations in local areas. In Figure 3 (b), the thickness of the B716 trumpet-shaped holes is 4–12 μm, with an average value of approximately 7.2 μm. The overall thickness is lower than that of the B716 circular holes, but the surface of the hole

wall shows local recast protrusions, indicating that there are certain molten product attachments in the trumpet-shaped area. Compared with B716, the recast layer of the B1503 group is thicker and has more pronounced morphology fluctuations. In Figure 3 (c), the thickness range of the B1503 circular holes expands to 5–44 μm, with an average value of approximately 16.3 μm. The measurement points of 28 μm, 44 μm, and 21 μm are concentrated in the local protrusions of the hole wall, indicating that a thicker recast deposition layer has formed at this location. In Figure 3 (d), the thickness of the B1503 trumpet-shaped holes is 6–24 μm, with an average value of approximately 12.3 μm. The recast layer of the hole wall also shows obvious fluctuations, with a local thickness reaching 24 μm. The results in Figure 3 indicate that the heat affected zone of the B1503 group has significantly stronger effects on the hole wall compared to B716, especially the maximum thickness of 44 μm in the B1503 circular holes, which shows a significant increase in local melting and recast deposition degree under this processing number. This phenomenon indicates that the morphology of the recast layer is not solely controlled by the hole shape, and the discharge conditions corresponding to the processing number will significantly change the thickness and uniformity of the recast layer on the hole wall.

To further compare the hole wall microstructure states of the two types of hole shapes under the final processing number, this paper observes the 500× microscopic structure photos of the B1902 group's circular holes and trumpet-shaped holes, as shown in Figure 4.

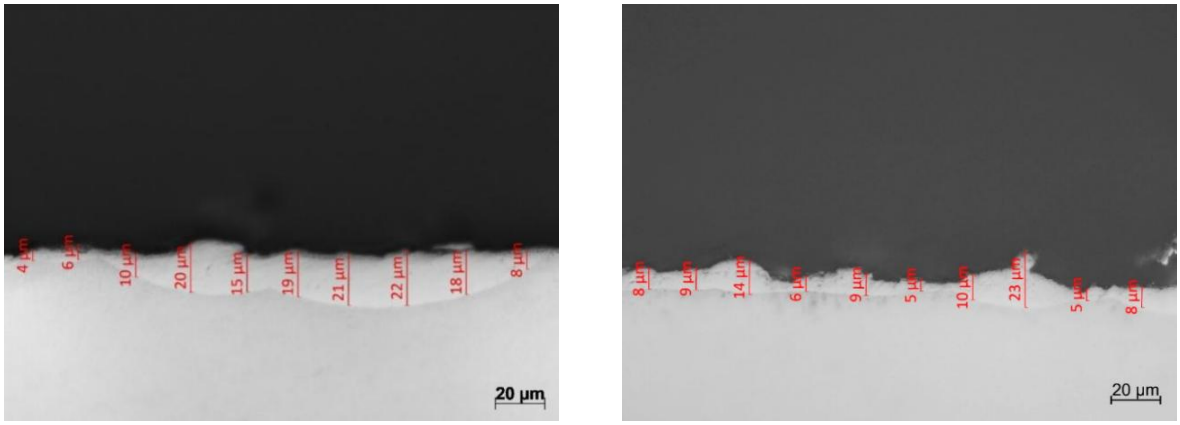

(a) B1902- Circular hole (b) B1902- Horn hole

Figure 4: Recast layer morphology of B1902 holes at 500×.

In Figure 4(a), the thickness marking value of the recast layer of the B1902 circular hole is 4-22 μm, with an average value of approximately 14.3 μm. There are several large thickness measurement points of 20 μm, 15 μm, 19 μm, 21 μm, 22 μm, and 18 μm in the middle of the hole wall, indicating that there is a wide continuous recast layer in this hole wall area. In Figure 4(b), the thickness range of the B1902 trumpet-shaped hole is 5-23 μm, with an average value of approximately 9.6 μm. The overall average thickness is lower than that of the circular hole, but the local maximum thickness reaches 23 μm, located in the local protrusion area on the right side of the hole wall, showing obvious local deposition characteristics. Compared with the B1503 group, the average thickness of the B1902 circular hole is still at a relatively high level, while the main feature of the B1902 trumpet-shaped hole is local peak protrusion and uneven overall thickness distribution.

In conclusion, the thickness differences of the recast layer of the DD9 single crystal superalloy hole walls under different processing numbers are significant. The recast layer of the B119 circular hole is the thinnest and most uniform, the B1503 circular hole shows the most severe local thickening, and the B1902 circular hole presents a wide continuous recast

layer. The trumpet-shaped holes in B119, B222, B1503, and B1902 all show different degrees of local undulation or peak thickening, indicating that the complex hole geometry enhances the non-uniformity of local recast on the hole wall. The overall results show that the recast layer of the DD9 single crystal superalloy hole walls after EDM processing is influenced by both the processing number and the hole shape. The maximum thickness and thickness fluctuation are more capable of reflecting the local thermal damage degree of the hole wall than the single average thickness.

3.2 Quantitative comparison of recast-layer thickness

In order to further compare the variation patterns of the recast layer thickness under different processing numbers and hole types, this paper has statistically summarized the thickness data of 10 measurement points in each group, as shown in Figure 5.

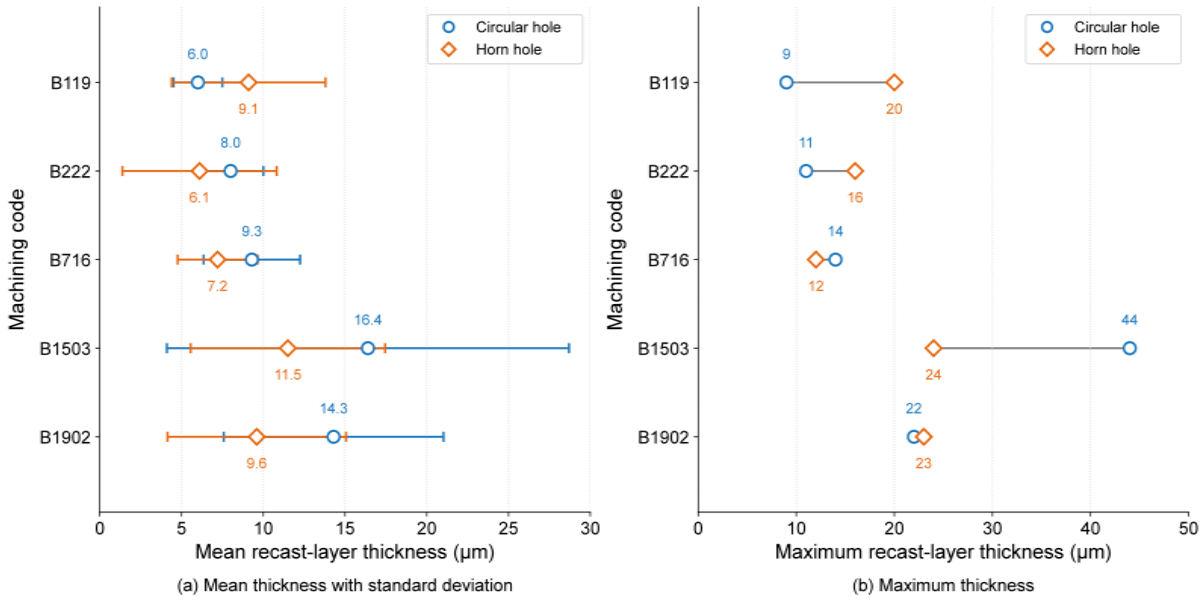

Figure 5: Quantitative comparison of mean and maximum recast-layer thickness under different machining codes.

As shown in Figure 5(a), the average recast layer thickness of the circular hole and the flared hole varies differently with the processing number. The average thickness of the circular hole increases from 6.0 μm in B119 to 16.4 μm in B1503, and remains at a relatively high level of 14.3 μm under the condition of B1902. The average thickness of the flared hole reaches 9.1 μm under the condition of B119, then drops to 6.1 μm and 7.2 μm in B222 and B716 respectively, and rises to 11.5 μm under the condition of B1503. Except for B119, the average thickness of the circular hole in B222, B716, B1503 and B1902 is higher than that of the flared hole, indicating that the overall thickening of the recast layer is not entirely determined by the geometry of the flared hole, and the discharge conditions corresponding to the processing number also play a major role. The standard deviation results further show that the thickness fluctuations of the circular hole in B1503 and B1902 are relatively large, reaching 12.30 μm and 6.72 μm respectively, indicating that the thickness distribution of the recast layer of these two groups of samples is less uniform.

As shown in Figure 5(b), the maximum recast layer thickness can better reveal the local thermal damage intensity. The maximum thickness of the circular hole in B1503 reaches 44 μm, which is the highest value among all samples, and is much higher than its average

thickness of 16.4 μm, indicating that there is a prominent local recrystallization deposition under this working condition. In the flared hole, the maximum thickness of B119, B1503 and B1902 reaches 20, 24 and 23 μm respectively, which are significantly higher than their respective average values, indicating that the main feature of the flared hole is not the continuous increase of the overall thickness, but that the local area of the hole opening or the hole wall is prone to peak thickening. Thus, the average thickness is suitable for evaluating the overall heat affected zone level, while the maximum thickness is more suitable for identifying the unstable local molten pool and concentrated re-deposition areas.

To further evaluate the uniformity of the recast layer thickness distribution, this paper uses the coefficient of variation and local instability index to conduct supplementary analysis of the data of each group. The dispersion degree and local instability characteristics of the recast layer thickness are shown in Figure 6.

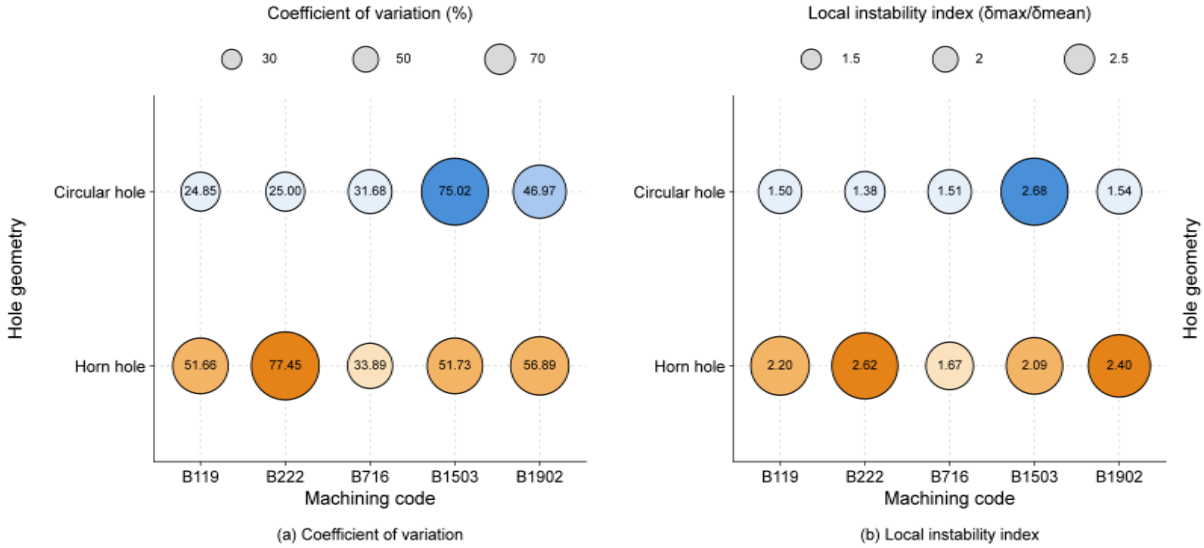

Figure 6: Thickness heterogeneity and local instability of the recast layer under different machining codes.

As shown in Figure 6(a), the coefficient of variation of the circular holes under conditions B119, B222, B716, B1503, and B1902 is 24.85%, 25.00%, 31.68%, 75.02%, and 46.97% respectively, while the coefficient of variation of the flared hole is 51.66%, 77.45%, 33.89%, 51.73%, and 56.89% respectively. The coefficient of variation of the flared hole in B222 is the highest, reaching 77.45%, indicating that the thickness fluctuation of the recast layer between different measurement points of this sample is the strongest. The coefficient of variation of the circular hole in B1503 is 75.02%, which corresponds to the maximum thickness of 44 μm in Figure 5, suggesting that the higher average value is mainly affected by the local abnormal thickening area. Figure 6(b) presents the local instability index, which is the ratio of the maximum thickness to the average thickness. The groups of circular holes are 1.50, 1.38, 1.51, 2.68, and 1.54 respectively, while those of the flared holes are 2.20, 2.62, 1.67, 2.09, and 2.40 respectively. The local instability index of the circular hole in B1503 is the highest, at 2.68; B222 and B1902 of the flared holes reach 2.62 and 2.40 respectively, showing obvious local thickness peaks.

In conclusion, the circular hole in B1503 exhibits the strongest thickening of the recast layer and local instability characteristics, while the flared hole in B222 exhibits the highest thickness dispersion. These results indicate that the recast layer after EDM machining of the DD9 single crystal superalloy does not form uniformly along the hole wall, and its thickness

distribution is affected by the processing number, hole geometry, melt product discharge, and local recrystallization behavior.

3.3 Mechanism of EDM-induced microstructural alteration in DD9 single-crystal superalloy

In order to explain the phenomena of thickening of the recast layer, amplification of local peaks, and enhancement of thickness fluctuations at the mechanism level, this paper further discusses these issues from three aspects: heat input, die geometry, and the response of single crystal materials. Firstly, the EDM process essentially belongs to a local transient thermal processing process. An increase in peak current, an extension of pulse width, or an increase in duty cycle will increase the heat input to the surface of the die, causing a deeper instantaneous molten pool near the discharge point. The molten metal can only be discharged in time under the action of the flushing liquid, and the remaining part will re-solidify and adhere to the die wall under a high cooling rate, thereby forming the recast layer. The significant differences in thickness levels and local peaks under different processing numbers are the direct manifestations of this difference in heat input. To verify the corresponding relationship between the enhancement of heat input and the aggravation of die wall damage, this paper conducts a combined analysis of the average recast layer thickness, the maximum thickness, and the thickness dispersion, as shown in Figure 7.

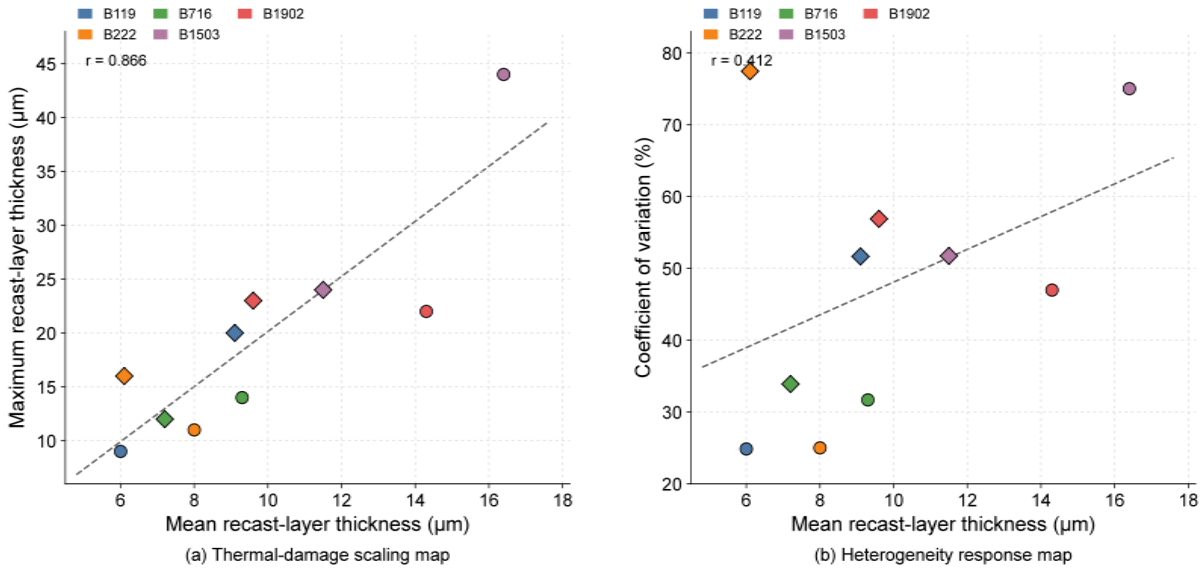

Figure 7: Thermal-damage scaling and heterogeneity response under different hole geometries.

As shown in Figure 7(a), the average thickness of the 10 samples has a significant positive correlation with the maximum thickness, with a correlation coefficient of 0.866, indicating that as the overall heat influence level increases, the local extreme thickness of the hole wall also increases simultaneously. Among them, the B1503 circular hole is located closest to the upper right area in the figure, with an average thickness of 16.4 μm and a maximum thickness of 44 μm, suggesting that under this working condition, the depth of the melt pool and the re-solidification accumulation are the most significant. Figure 7(b) shows that the average thickness and the coefficient of variation also show a positive trend of change, with a correlation coefficient of 0.412. Although the correlation degree is weaker than that in Figure 7(a), it can be observed that the B222 trumpet-shaped hole, B1902 trumpet-shaped hole, and

B1503 circular hole are all in the higher dispersion area, indicating that the thickness of the remelting layer is not only controlled by the average heat input, but also closely related to the local chip removal conditions and the instantaneous discharge stability near the hole wall.

Secondly, the hole geometry will change the discharge channel and the liquid flow field, thereby affecting the discharge path of the molten product and the deposition position of the backflow. The channel cross-section of the circular hole is relatively stable, and the heating on the hole wall is relatively uniform. While the trumpet-shaped hole is more prone to local gap changes and flow field disturbances in the expansion area of the hole opening, which then induces secondary discharge and the backflow of molten metal. Figure 8 further presents the geometric response difference of the trumpet-shaped hole relative to the circular hole.

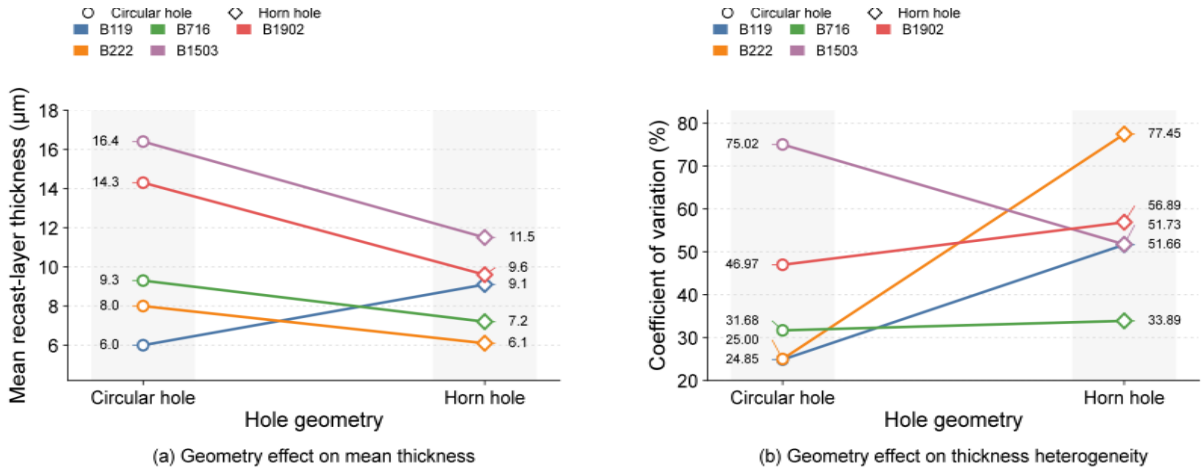

Figure 8: Geometric effect of flared-hole configuration on mean thickness and thickness heterogeneity.

As shown in Figure 8(a), the influence of the flared hole on the average recast layer thickness is not uniform. In B119, the flared hole increases the thickness by 3.1 μm, while in B222, B716, B1503, and B1902, it decreases by 1.9, 2.1, 4.9, and 4.7 μm respectively. This indicates that the flared structure does not necessarily lead to an overall increase in the recast layer thickness. Its effect is more dependent on the stability of discharge under specific processing parameters. Figure 8(b) shows that the flared hole has a more prominent effect on the thickness dispersion. Except for B1503, the differences in the coefficient of variation for the other four groups are all positive. Among them, B222 reaches +52.45%, and B119 reaches +26.81%. This means that although the flared hole may not necessarily bring a higher average thickness, it is more likely to form a recast layer with uneven spatial distribution, presenting characteristics such as local thickening, local thinning, and shift of the peak position.

Finally, as a single crystal superalloy, the micro-damage mechanism of DD9 is also constrained by the inherent microstructure of the material. Although this material does not have the problem of grain boundary weakening as in conventional polycrystalline alloys, the γ/γ' phase structure, dendrite segregation, and the local distribution of strengthening elements such as Al, Ti, Ta, and W will affect the formation process of the melting initiation position and the re-solidification interface. The recast layer after rapid solidification may retain certain epitaxial solidification characteristics, but the increased dislocation density, enhanced element segregation, oxidation inclusions, and microcrack initiation will significantly weaken the surface integrity of the hole wall. For gas film holes or irregular cooling holes, these surface defects will become weak links in subsequent high-temperature service. Existing studies have shown that introducing a grinding fluid flow after EDM or laser drilling can help thin or remove the recast layer and can increase the creep rupture time of the sample from 119.64 h to

136.15 h, an increase of approximately 13.8%. Combining the results of this study, it can be concluded that the EDM drilling quality of DD9 single crystal superalloy is not solely determined by the removal efficiency, but is controlled by the heat input intensity, the local discharge behavior induced by the hole shape, and the response of the single crystal structure. Therefore, in process optimization, the pulse energy, discharge stability, and the subsequent surface integrity of the hole area should be controlled simultaneously to reduce the thickness of the recast layer and its unevenness.

4 Conclusion

This paper conducts an experimental analysis on the recast layer and microstructure damage on the hole wall after EDM drilling of DD9 single crystal superalloy. A micro observation, image calibration and multi-point thickness measurement process for the recast layer after EDM drilling of DD9 single crystal superalloy is established. Based on the 2404554MICRO01 to 2404554MICRO05 series samples, a comparative analysis was conducted on the round holes and trumpet-shaped holes under five processing numbers (B119, B222, B716, B1503, and B1902). This enables more clear data support for the evaluation of the hole wall microstructure. The main findings of this research are as follows:

(1) The EDM responses of round holes and trumpet-shaped holes are different. Round holes can better reflect the state of the recast layer in the relatively stable hole wall area; trumpet-shaped holes are more likely to show local re-deposition, thickness fluctuations, and enhanced thermal influence at the hole opening due to expansion, changes in local discharge gaps, and fluid disturbance. Therefore, these two types of hole shapes need to be evaluated separately.

(2) The average recast layer thickness, maximum thickness, coefficient of variation, and microcrack density can be used as core indicators for evaluating the quality of EDM drilling of DD9 single crystal superalloy. The average thickness reflects the overall thermal influence level, while the maximum thickness and coefficient of variation are more suitable for identifying local instability of the molten pool and re-solidification accumulation.

(3) This paper provides experimental basis for the EDM process optimization of DD9 single crystal blade gas film holes, micro holes, and special-shaped holes. In the future, combined with SEM, EDS, EBSD, microhardness, and post-processing with abrasive flow experiments, the relationship between EDM parameters, hole wall microstructure integrity, and high-temperature service performance can be further established.

About the Author

Shuai Zheng is a male Han Chinese Senior Engineer from Baoding, Hebei Province, China. He holds a master’s degree, and his research focuses on the development of high-temperature alloy blades.

Yulan Zhu is a female Han Chinese Engineer from Henan Province, China. She holds a doctoral degree, and her research focuses on electrical discharge machining of holes in high-temperature alloys.

References

[1] Yang, J., Liu, Y., Sun, D., et al. (2023). Revealing the formation of recast layer around the film cooling hole of single-crystal superalloy. Metals, 13(4), 695. DOI:

10.3390/met13040695.

[2] Alkahlan, M. A., Pervaiz, S., Anwar, S., et al. (2023). Formation and characterization of the recast layer formed on Inconel 718 during wire electrical discharge machining. Materials, 16(3), 930. DOI: 10.3390/ma16030930.

[3] Kar, A., Gupta, K., & Sahoo, S. (2025). Optimizing WEDM parameters in Inconel 718 using a hybrid MEREC–CRITIC–CoCoSo approach. Scientific Reports, 15, 33947. DOI: 10.1038/s41598-025-11188-3.

[4] Gokcekaya, O., Su, Y., Ishimoto, T., Nakano, T., & Gupta, M. K. (2024). Wire-EDM performance and surface integrity of Inconel 718 with unique microstructural features fabricated by laser powder bed fusion. The International Journal of Advanced Manufacturing Technology, 130, 4513–4528. DOI: 10.1007/s00170-023-12924-7.

[5] Seidi, M., Gohari, S., Kordkheili, S. A. H., & Ebrahimi, R. (2024). Multi-objective optimization of the wire electrical discharge machining process using multi-attribute decision-making techniques and regression analysis. Scientific Reports, 14, 10234. DOI: 10.1038/s41598-024-60825-w.

[6] Raj, A., Bisaria, H., & Shandilya, P. (2023). Performance analysis of WEDM during the machining of Inconel 690 miniature gears using RSM and ANN modeling approaches. Reviews on Advanced Materials Science, 62(1), 20220288. DOI: 10.1515/rams-2022-0288.

[7] Karthikeyan, S., Gowthaman, S., Vinoth Kumar, K., et al. (2025). Influence of WEDM input variables on the machinability of Ni–Cu superalloy. Materials and Manufacturing Processes, 40, online article. DOI: 10.1080/10426914.2024.2406781.

[8] Raj, A., Bisaria, H., & Shandilya, P. (2024). Design, modeling, and parametric optimization of WEDM of Inconel 690 using the RSM-GRA approach. International Journal on Interactive Design and Manufacturing, 18, 2107–2117. DOI: 10.1007/s12008-022-00947-5.

[9] Ming, W., Shen, F., Zhang, G., et al. (2023). Optimization of process parameters and performance for machining Inconel 718 in renewable dielectrics. Alexandria Engineering Journal, 79, 164–179. DOI: 10.1016/j.aej.2023.07.075.

[10] Patel, B., Gohel, P., & Makhesana, M. A. (2023). Machining of nickel-based superalloy Inconel 718 using alumina nanofluid in powder-mixed electric discharge machining. Materials Research Express, 10(3), 036501. DOI: 10.1088/2053-1591/acbae8.

[11] Patil, A., Urkude, N., Gupta, S., & Rashid, M. (2023). Surface roughness and topography of EDM machining of Inconel 718. Materials Today: Proceedings. DOI: 10.1016/j.matpr.2023.02.444.

[12] Selvarajan, L., Rajkumar, K., & Rajan, T. P. D. (2024). Optimization of electrical discharge machining parameters for enhanced performance on Inconel 718 using Cu-Ni-B4C nanocomposite electrodes and advanced modeling techniques. Materials Research Express, 11(9), 095004. DOI: 10.1088/2053-1591/ad755d.

[13] Bhowmick, S., Sarkar, B. R., & Biswas, N. (2023). Parametric optimization and prediction of MRR and surface roughness of titanium mixed EDM for Inconel 718 using RSM and fuzzy logic. CIRP Journal of Manufacturing Science and Technology, 40, 10–28. DOI: 10.1016/j.cirpj.2022.11.002.

[14] Paswan, D., Singh, N. K., Kumar, A., et al. (2023). An analysis of microstructural morphology, surface topography, surface integrity, recast layer, and machining performance of graphene nanosheets on Inconel 718 superalloy. Journal of Materials Research and Technology, 27, 7138–7158. DOI: 10.1016/j.jmrt.2023.11.080.

[15] Nakano, Y., Okada, A., & Okamoto, Y. (2023). Wire electrochemical finishing of wire electrical discharge machined surfaces of highly alloyed materials with insoluble precipitates. Journal of Materials Processing Technology, 313, 117863. DOI: 10.1016/j.jmatprotec.2023.117863.

[16] Straka, Ľ., Hašová, S., Pitel, J., et al. (2024). Assessment of surface integrity in precision electrical discharge machining of HSS EN HS6-5-2C. Micromachines, 15(12), 1469. DOI: 10.3390/mi15121469.

[17] Nowicki, D., & Świercz, R. (2025). Microstructural analysis of recast layer thickness and microcrack formation during EDM of Hastelloy C-22 with different graphite electrodes. Materials, 18(23), 5338. DOI: 10.3390/ma18235338.

[18] Adnan, M., Ramesh, S., & Kumar, P. (2025). Tribology of EDM recast layers vis-à-vis TIG cladding coatings: An experimental investigation. Micromachines, 16(8), 913. DOI: 10.3390/mi16080913.

[19] Zhang, Y., Li, W., Chen, X., et al. (2025). Recast layer-induced fatigue degradation in high-speed EDM microholes: Experimental characterization. Materials, 18(9), 1985. DOI: 10.3390/ma18091985.

[20] Wang, Y., Zhang, Z., Wang, L., et al. (2025). Effect of shaped film cooling hole manufacturing defects on the high-cycle fatigue behavior of a Ni-based single-crystal superalloy. Fatigue & Fracture of Engineering Materials & Structures, 48(7), 2803–2820. DOI: 10.1111/ffe.14641.

[21] Zhang, D., Liu, X., Wang, Y., et al. (2024). Temperature–stress coupling fatigue behavior of film-cooling holes in complex temperature fields. Materials, 17(15), 3785. DOI: 10.3390/ma17153785.

[22] Zhang, Z., Wang, L., Xu, J., et al. (2024). Improving the fatigue property of diffusive film cooling holes in nickel-based single crystal superalloy via ultrashort pulse laser drilling coupled with abrasive flow machining. Journal of Materials Processing Technology, 328, 118411. DOI: 10.1016/j.jmatprotec.2024.118411.

[23] Wang, L., Wang, Z., Xu, J., Zhao, W., & Zhang, Z. (2025). Towards manufacturing high-quality film-cooling holes using femtosecond laser combined with abrasive flow. Micromachines, 16(9), 973. DOI: 10.3390/mi16090973.

[24] Li, P., Liu, X., Zhang, J., et al. (2025). Microstructure evolution and damage mechanism of the DD9 single-crystal superalloy-thermal barrier coating system under

high-temperature oxidation: A comparative study with DD6. Materials, 18(18), 4332. DOI: 10.3390/ma18184332.

[25] Xue, Y., Zhang, J., Liu, L., et al. (2023). Effect of withdrawal rate on solidification microstructures of a DD9 single-crystal superalloy turbine blade. Materials, 16(9), 3409. DOI: 10.3390/ma16093409.